

Monolithic Nanoporous Copper ribbons from Mg-Cu Alloys with Copper Contents below 33 at. %: Fabrication, Structure Evolution and Coarsening Behavior along the Thickness Direction

Wenbo Liu^{1,2}, Shichao Zhang^{1,*}, Ning Li², Jiwei Zheng¹, ShenShen An¹, and Yalan Xing¹

¹ School of Materials Science and Engineering, Beihang University, Beijing 100191, China

² School of Manufacturing Science and Engineering, Sichuan University, Chengdu 610065, China

*E-mail: liuwenbo_8338@163.com, csc@buaa.edu.cn

Received: 11 September 2011 / *Accepted:* 18 October 2011 / *Published:* 1 November 2011

Monolithic nanoporous copper (NPC) ribbons with unimodal or bimodal channel size distributions can be fabricated through chemical dealloying of Mg-Cu alloys with Cu content below 33 at.% in an acidic solution at room temperature. The microstructure of these NPC ribbons was characterized using X-ray diffraction, scanning electron microscopy, energy dispersive X-ray analysis, transmission electron microscopy, and high-resolution transmission electron microscopy. The experimental results show that with increasing Cu content from 13.5 at.% up to 32 at.%, NPC with unimodal channel size distributions gradually changes into that with bimodal channel size distributions upon the dealloying; meanwhile we found cracking to be unavoidable. For the Mg-Cu alloys composed of α -Mg and Mg₂Cu, the microstructure of the NPC ribbons strongly depends upon phase proportions and distributions in the initial alloys. The Mg-Cu alloys with 13.5-25 at.% Cu can be fully dealloyed and result in the formation of NPC with a homogenous structure, while the separate dealloying of α -Mg and Mg₂Cu in the Mg-32 Cu alloy leads to the formation of NPC with bimodal pore size distributions. Moreover, the microstructures of two distinct surfaces of the NPC ribbon from the Mg-32 Cu alloy make an essential difference due to the great disparity in the phase distributions, which can be attributed to the different cooling rates on the free and quenching surfaces during rapid solidification. In addition, the evolution process of porous structure along the thickness direction of alloy ribbons during the dealloying is from the interior to exterior, which is just contrary to the coarsening process during the post-dealloying. The evolution and coarsening mechanisms are discussed in detail based upon percolation theory and chloride ion effect.

Keywords: Nanoporous copper; Dealloying; Acid corrosion; Evolution; Coarsening

1. INTRODUCTION

Nanoporous metals (NPMs), as novel functional materials, have attracted considerable interest in a wide variety of applications including catalysis, sensors, actuators, fuel cells, microfluidic flow controllers, and so forth [1-4].

For a long time past, template methods are commonly used to fabricate these materials through the replication of porous alumina or liquid-crystal templates [5-7]. Since it has been found that dealloying can be used to yield a broad range of porous metals, during the latest decades, a great deal of effort has been directed towards the investigation of NPMs prepared through dealloying [8-11]. Until now, most of the reported porous metals were fabricated by dealloying from single-phase solid solution alloy systems, which refers to the selective dissolution of one or more active components from an alloy, such as Cu-Pt, Ag-Au, Cu-Au and Au-Ag-Pt [12-15].

In view of their industrial applications, widespread uses of the dealloying technique to make NPMs are frequently hindered by the high cost of these noble metals and the alloy systems limited. Thus, the fabrication of nanoporous materials from the alloy families based on common metals with multiple phases urgently needs to be investigated.

Lu et al. [16] have reported that porous copper with a significantly large channel size can be synthesized from nanocrystalline two-phase Cu-Zr films by electrochemical dealloying, but no porous structure can be obtained from the as-cast Cu-Zr alloys under the same conditions. Still, few substantial researches have thus far focused on this topic using electrochemical/chemical dealloying technique, due to the difficulties in clarifying the dealloying behavior and controlling the dissolution process among the different phases [17].

Recently, Zhang et al. [18] also claimed the monolithic NPC can be achieved by chemical dealloying of dual-phase Mg-Cu alloys with 33-67 at.% Cu in the HCl solution in virtue of the synergetic dealloying between Mg₂Cu and MgCu. Henceforth, Mg-Cu system can serve as a new candidate to fabricate the monolithic NPC due to the large standard reversible potential difference between Mg and Cu (-2.375 V standard hydrogen electrode (SHE) for Mg/Mg²⁺ and 0.342 V SHE for Cu/Cu²⁺); however, no further studies have been conducted on the alloy system with other composition ranges.

Based upon the binary Mg-Cu alloy phase diagram [19], it can be expected that the dealloying behavior and porosity evolution of the Mg-Cu alloys with copper content below 33 at.% are significantly different from those of the Mg-Cu alloys in the literature due to the great disparity in phase constituents and distributions of the initial alloys. Here, we show that monolithic NPC ribbons with single modal or bimodal pore size distributions can be fabricated through chemical dealloying of Mg-Cu alloys with Cu contents below 33 at.% in an acidic solution at room temperature. For these Mg-Cu alloys composed of α -Mg and Mg₂Cu, the microstructures of the NPC ribbons strongly depend upon the phase proportions and distributions in the initial alloys. Additionally, the evolution/coarsening process of porous structure along the thickness direction of the ribbons during the dealloying/post-dealloying has been investigated, and the corresponding mechanism is discussed in detail.

2. EXPERIMENTAL SECTION

Mg-Cu alloys with nominal compositions of 13.5, 14.5, 15.5, 25, 32 at.% Cu were prepared from pure Mg (99.9 wt.%) and pure Cu (99.999 wt.%). Voltaic arc heating was employed to melt the charges in a copper crucible under an argon atmosphere, and then the melt was cooled down into ingots in situ. By use of a single roller melt spinning apparatus, the ingots were remelted in a quartz tube by high-frequency induction heating and then melt-spun onto a copper roller at a circumferential speed of ~3000 rpm in a controlled argon atmosphere. The ribbons obtained were typically 20-40 μm in thickness, 4-6 mm in width, and several centimeters in length. The dealloying of the rapidly solidified (RS) Mg-Cu ribbons was performed in a 1 wt.% HCl aqueous solution at room temperature (RT) until no obvious bubbles emerged. The typical dealloying duration ranged from 5min to 30min dependent upon the thickness of the ribbons and alloy compositions. After dealloying, the samples were rinsed with distilled water and dehydrated alcohol. The as-dealloyed samples were kept in a vacuum chamber to avoid oxidation.

The phases present in the RS Mg-Cu alloys and as-dealloyed samples were identified using an X-ray diffractometer (XRD, Rigaku D/Max-2400) with Cu $K\alpha$ radiation. The free surface (contacting with the air), quenching surface (contacting with the copper roller), and cross sections of the NPC ribbons were observed using a scanning electron microscope (FESEM, Hitachi S-4800). The chemical compositions of the NPC ribbons were determined using an energy dispersive X-ray (EDX) analyzer, which is attached to FESEM. The microstructures of the NPC ribbons were also characterized using a transmission electron microscope (TEM, JEOL JEM 2100F) with selected-area electron diffraction (SAED) and a high-resolution TEM (HRTEM, JEOL JEM 2100F).

To test the electrochemical activities of α -Mg and Mg_2Cu phases in the RS Mg-Cu alloys, potentiodynamic polarizations studies were conducted on single-phase α -Mg solid solution and Mg_2Cu intermetallic compound in the 1 wt.% HCl solution at RT by using an electrochemical measurement unit (PARSTAT 2273). The experiments were carried out in a standard three-electrode electrochemical cell (200mL) with a Pt plate electrode as a counter electrode, a saturated calomel electrode (SCE) as a reference electrode, and the alloy ribbon as the working electrode. Polarization scan was performed towards positive values at a scan rate of 1.0 mV s^{-1} , after allowing a steady state potential to develop.

3. RESULTS AND DISCUSSION

Figure 1A shows the XRD patterns of the initial RS Mg-Cu alloy ribbons. The filled circles and squares in Figure 1A stand for α -Mg and Mg_2Cu , respectively. All the Mg-Cu alloys are composed of two distinct phases: α -Mg solid solution and Mg_2Cu intermetallic compound. With increasing Cu content in the initial alloys, the amount of α -Mg decreases, but that of Mg_2Cu increases, as indicated by the variation of diffraction peak intensities in Figure 1A. For the RS Mg-Cu alloys with 13.5, 14.5, 15.5 at.% Cu, the amount of α -Mg is nearly comparable to that of Mg_2Cu . When the Cu content is more than 15.5 at.% in the initial alloys, the diffraction peak intensities of the Mg_2Cu phase are

significantly stronger than those of the α -Mg phase, suggesting that the Mg_2Cu phase has turned out to be the main part in the initial alloys.

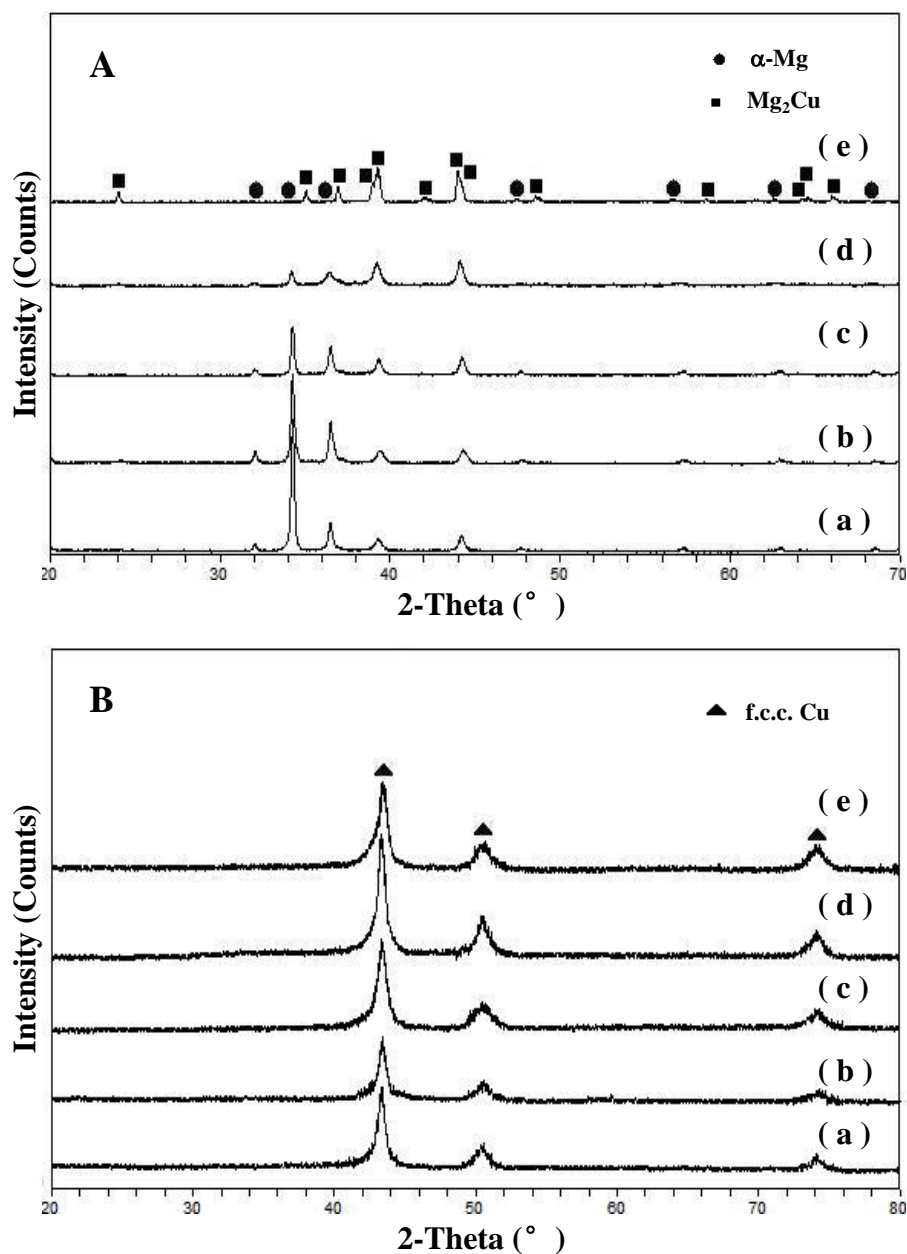
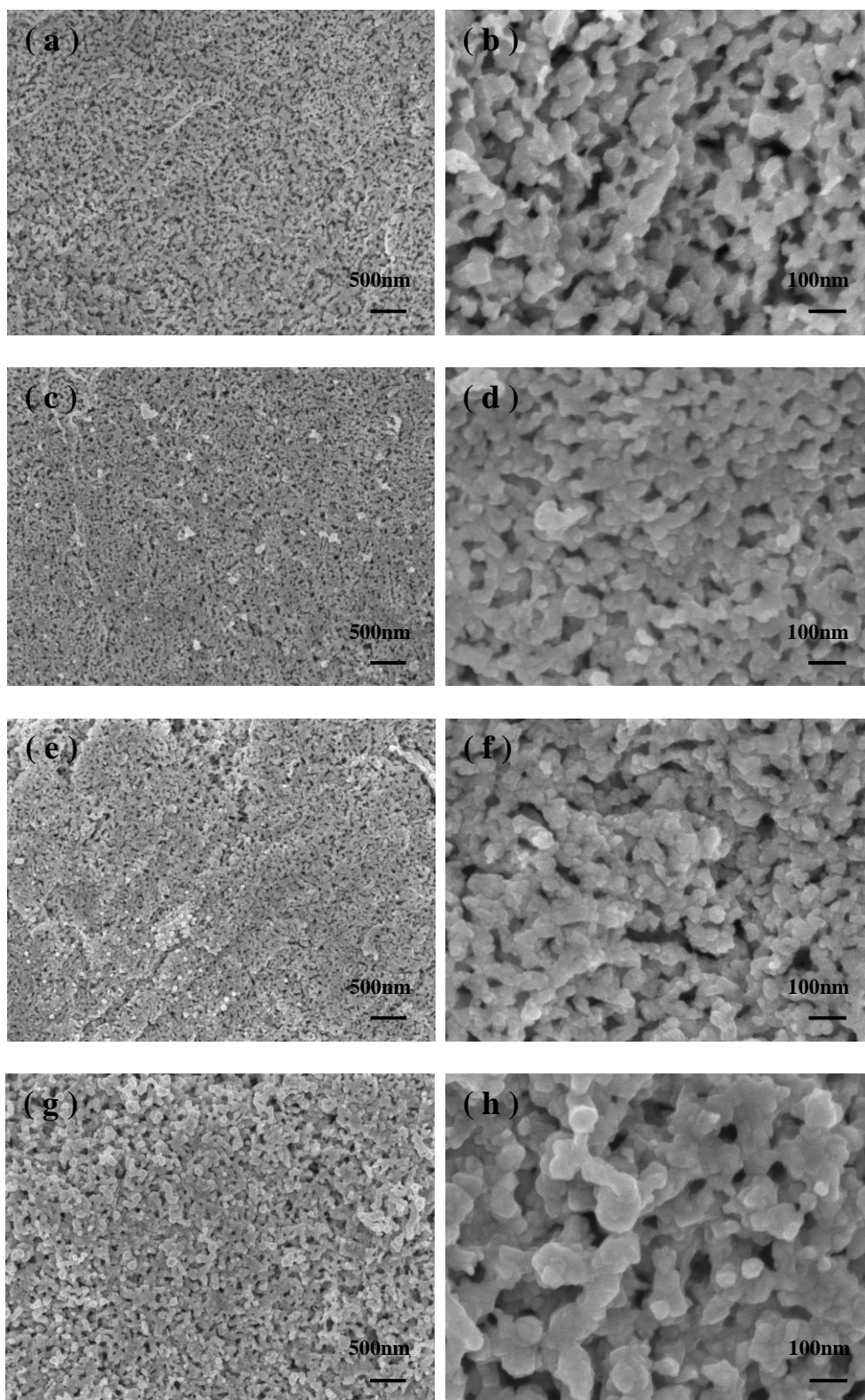


Figure 1. XRD patterns of RS Mg-Cu alloy ribbons (A) before and (B) after dealloying. (a-e) Mg-13.5, 14.5, 15.5, 25, and 32 Cu, respectively.

With increasing Cu content up to 25 at.%, it is obvious that the Mg_2Cu phase is dominant. When the Cu content reaches 32 at.%, only a minor amount of α -Mg can be detected in the alloys. In addition, on a basis of the phase diagram,¹⁹ it can be known that the Mg-13.5 Cu alloy is hypoeutectic structure, the Mg-14.5 Cu alloy eutectic structure, and the Mg-Cu alloys with 15.5-32 at.% Cu

hypereutectic structures. After dealloying of all the RS Mg-Cu alloys, only a face-centered cubic (f.c.c.) Cu phase can be identified in the as-dealloyed samples (Figure 1B).



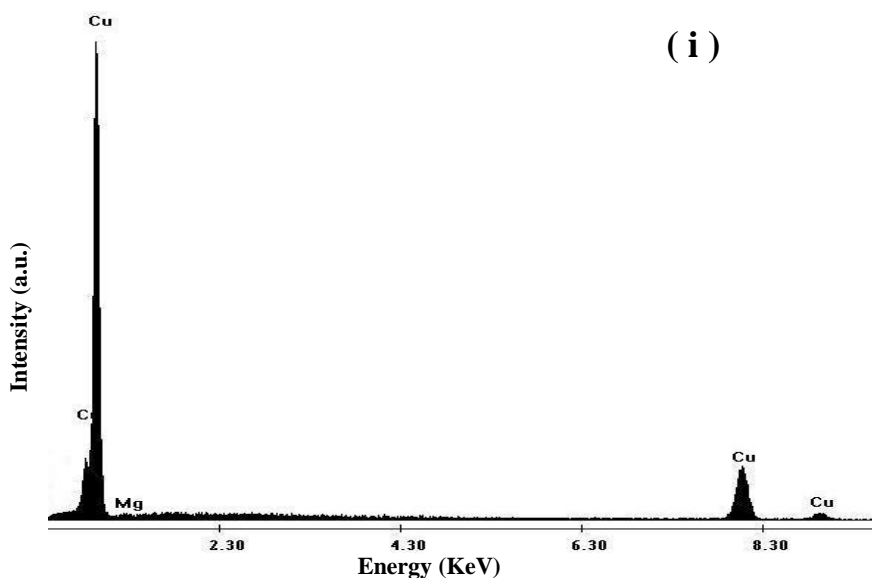


Figure 2. SEM images showing the microstructure of NPC by dealloying of (a-b) Mg-13.5 Cu, (c-d) Mg-14.5 Cu, (e-f) Mg-15.5 Cu, (g-h) Mg-25 Cu alloys in the 1 wt.% HCl solution at RT. Parts b, d, f and h are the high-magnification images. (i) EDX spectrum of NPC by dealloying of the Mg-25 Cu alloy. a.u.: arbitrary units.

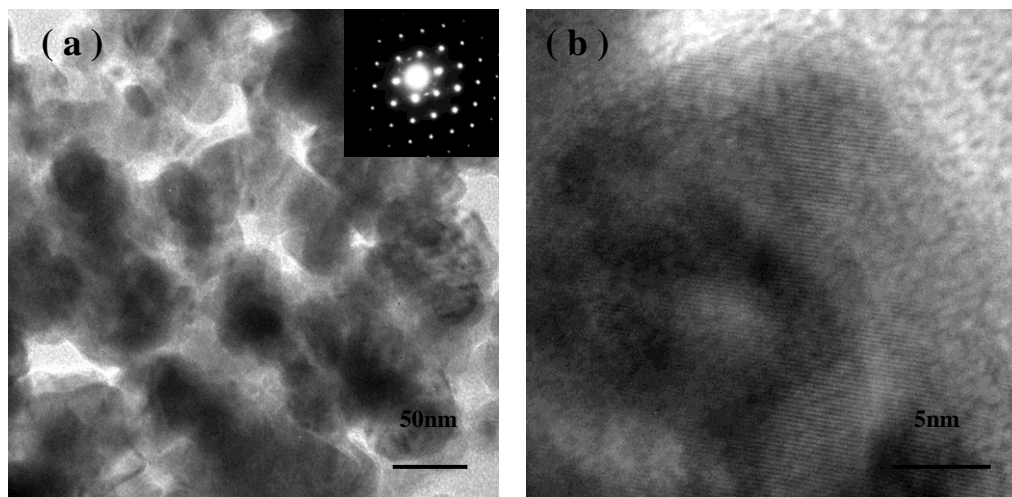
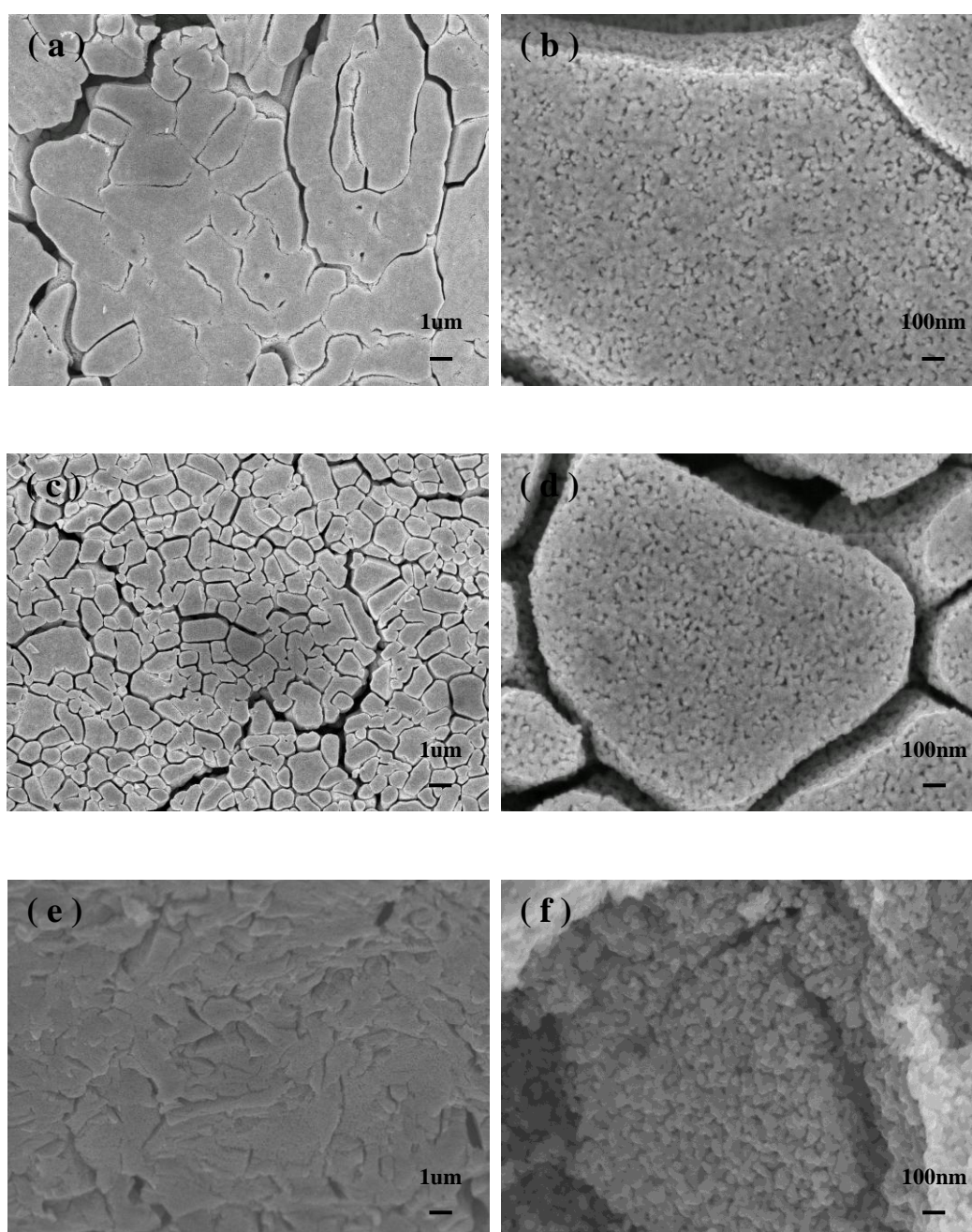


Figure 3. (a) TEM image showing the porous structure of NPC by dealloying of the Mg-25 Cu alloy in the HCl solution. (Inset) SAED pattern corresponding to one ligament in part a. (b) HRTEM image showing lattice fringes extending throughout this ligament.

Figure 2 shows the porous structure of NPC upon dealloying of RS Mg-13.5, 14.5, 15.5, and 25 Cu alloy ribbons in the HCl solution. It is clear that the as-dealloyed ribbons exhibit an open, three-dimensional (3D) bicontinuous interpenetrating ligament-channel structure with single modal channel size distributions and with the increase of Cu content in the initial alloys, the length scales of ligaments/channels in the NPC ribbons varies from 50 ± 10 nm (for Mg-13.5 Cu) to 100 ± 20 nm (for Mg-25 Cu). Analogically, we can also decrease the length scales of ligaments/channels in NPC by

decreasing the Cu concentration in the RS Mg-Cu alloys. There is a lower limit of the Cu concentration, however, below which the structures will collapse and the shape of the ribbons cannot be preserved. For example, the dealloying of a RS Mg-10 Cu alloy results in the formation of NPC powders (like Raney metals [20]) instead of monolithic ribbons (not shown here). EDX analysis has been performed on all the NPC ribbons, and one typical spectrum is shown in Figure 2i. It is obvious that all of Mg is removed from the Mg-Cu alloys during dealloying. In contrast, NPG by dealloying of Ag-Au alloys normally contains some at.% residual Ag. The residual Ag is expected to be trapped inside the Au ligaments based on the dealloying mechanism [21,22]. Also, the residual Ag cannot be totally removed but asymptotically reaches a limit at exhaustively long etching times (up to 100 h) [21].



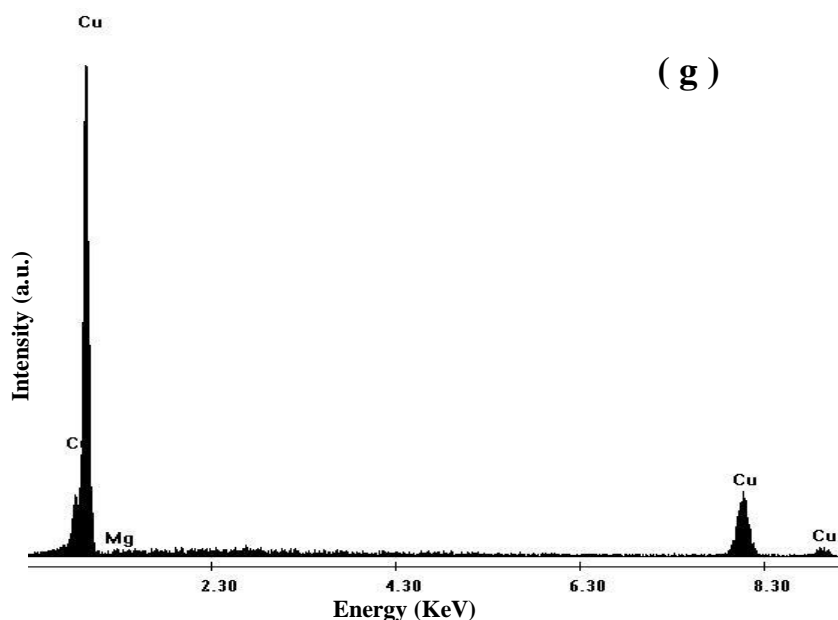


Figure 4. SEM images showing the microstructure of (a, b) free surface, (c, d) quenching surface, and (e, f) cross-section of the NPC ribbons by dealloying of the RS Mg-32 Cu alloy in the HCl solution for 15 min. (a, c, e) Low-magnification images. (b, d, f) High-magnification images. The large-sized channels can be clearly seen in parts a, c, and e. The High-magnification images show the nanoporous structure of the channel walls in NPC. (g) A typical EDX spectrum shows the composition of NPC.

In addition, TEM observation further verifies the porous structure of the NPC ribbons and one typical TEM bright-field image is shown in Figure 3a. A SAED pattern of one ligament shows a hexagonal pattern, which is from the face-centered cubic (f.c.c.) Cu [110] zone axis, indicating a single crystalline characteristic of the selected area (inset of Figure 3a). Moreover, the lattice fringes can be seen extending throughout this ligament (Figure 3b). It should be noted, however, the present results are essentially different from the established notion that the crystal lattice orientation is retained during dealloying of Ag-Au alloys with the conservation of the grain size of the master alloys [23-26]. For the lattice structure of the resulting NPC is considerably different from that of α -Mg or Mg_2Cu in the initial Mg-Cu alloy (α -Mg: solid solution; Mg_2Cu : face-centered orthorhombic; Cu: f.c.c.).

The plane view of the NPC ribbons from Mg-32 Cu alloy shows that a porous structure with bimodal channel size distributions can be obtained upon the dealloying in the HCl solution for 15min and typical SEM images of the free and quenching surfaces of the NPC ribbons are shown in Figure 4a-d. Part a of Figure 4 shows the SEM image of the free surface of the NPC ribbons. The free surface exhibits a porous structure with length scales of hundreds of nanometers; it should be noted that, however, these large-sized channels are not cracks, although like them. The SEM image at a higher magnification shows that the channel walls exhibit an open, bicontinuous interpenetrating ligament-channel structure with length scales of 10-20 nm (Figure 4b). The quenching surface of the NPC ribbons is porous but its morphology is obviously different from that of the free surface (Figure 4c), while the channel walls are also nanoporous, similar to those of the free surface (Figure 4d). The

section view of the NPC ribbons shows that the large-sized channels (hundreds of nm) penetrate the whole ribbons and a typical SEM image is shown in Figure 4e. The fracture surface of the channel wall of the NPC ribbons clearly exhibits an open, bicontinuous interpenetrating ligament-channel structure, suggesting that the nanoporous structure of the channel walls is 3D (Figure 4f). The walls of some large-sized channels form island-shaped structures and one typical counterpart is exhibited in part d of Figure 4. It is reasonable to assume that the morphology and size of these island-shaped structures in NPC inherit from the Mg_2Cu grains in the initial Mg-32 Cu alloy. Obviously, the NPC ribbons have bimodal channel size distributions composed of large-sized channels (hundreds of nm) with highly porous channel walls (tens of nm). Both large- and small-sized channels are 3D, open and bicontinuous. EDX analysis has been performed on the free, quenching surfaces and the cross-section of the NPC ribbons, and one typical spectrum is shown in Figure 4g. Clearly, only Cu can be identified and all of Mg is removed from both surfaces and interior of the Mg-32 Cu alloy ribbons during dealloying.

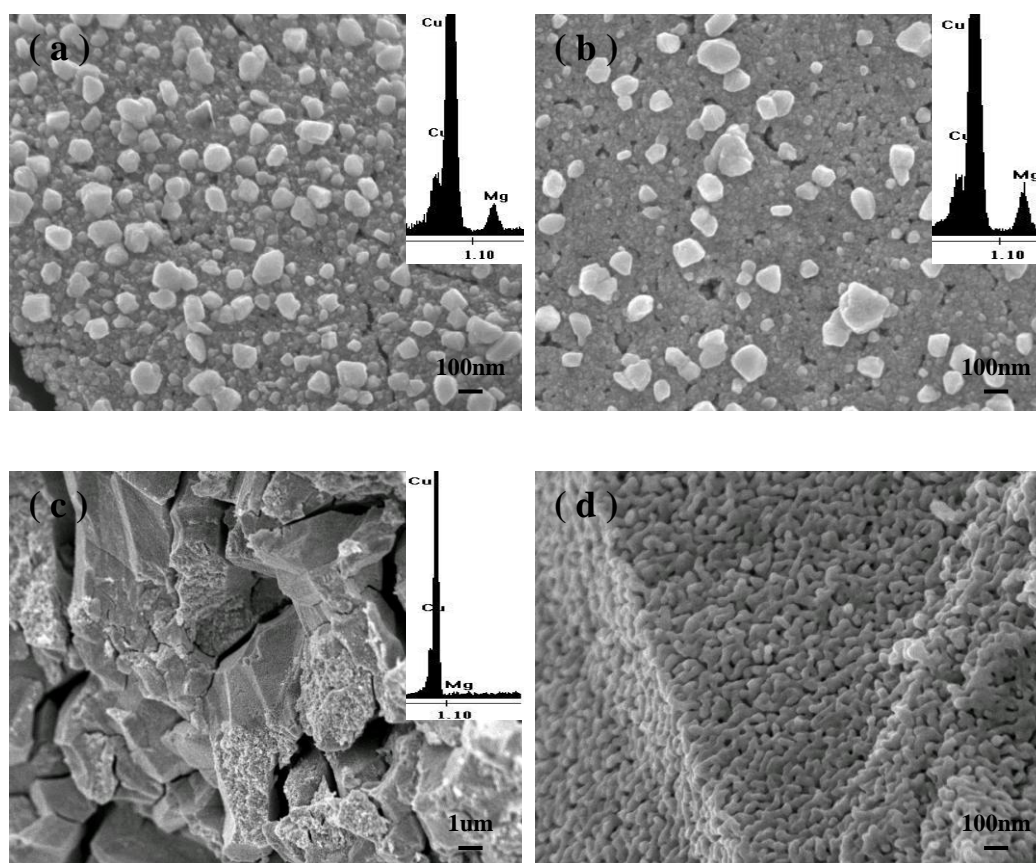


Figure 5. SEM images showing the microstructure of (a) free surface, (b) quenching surface, and (c, d) cross-section of the NPC ribbons by dealloying of the RS Mg-32 Cu alloy in the HCl solution for 10 min. (d) High-magnification image corresponding to part c. The insets show the corresponding EDX spectra.

In order to investigate the evolution process of porous structure along the thickness direction of the alloy ribbons during the dealloying, the RS Mg-32 Cu alloy is taken as an example. Figure 5 shows the microstructure of the surface and cross-section of as-dealloyed samples upon the dealloying for 10

min. Clearly, no noticeable porous structure can be observed from the surface of ribbons, while a well-evolved one has been formed in the inner space. EDX analysis has been performed and typical spectra show that nearly all of Mg is removed from the interior of ribbons, while a relatively high at.% residual Mg can be detected on the surface of samples upon the dealloying (insets of Figure 5a-c). The present results indicate that the evolution process of porous structure along the thickness direction of ribbons during the dealloying is from the inside to the outside, suggesting that the formation of the porous network on the surface obviously falls behind that in the interior.

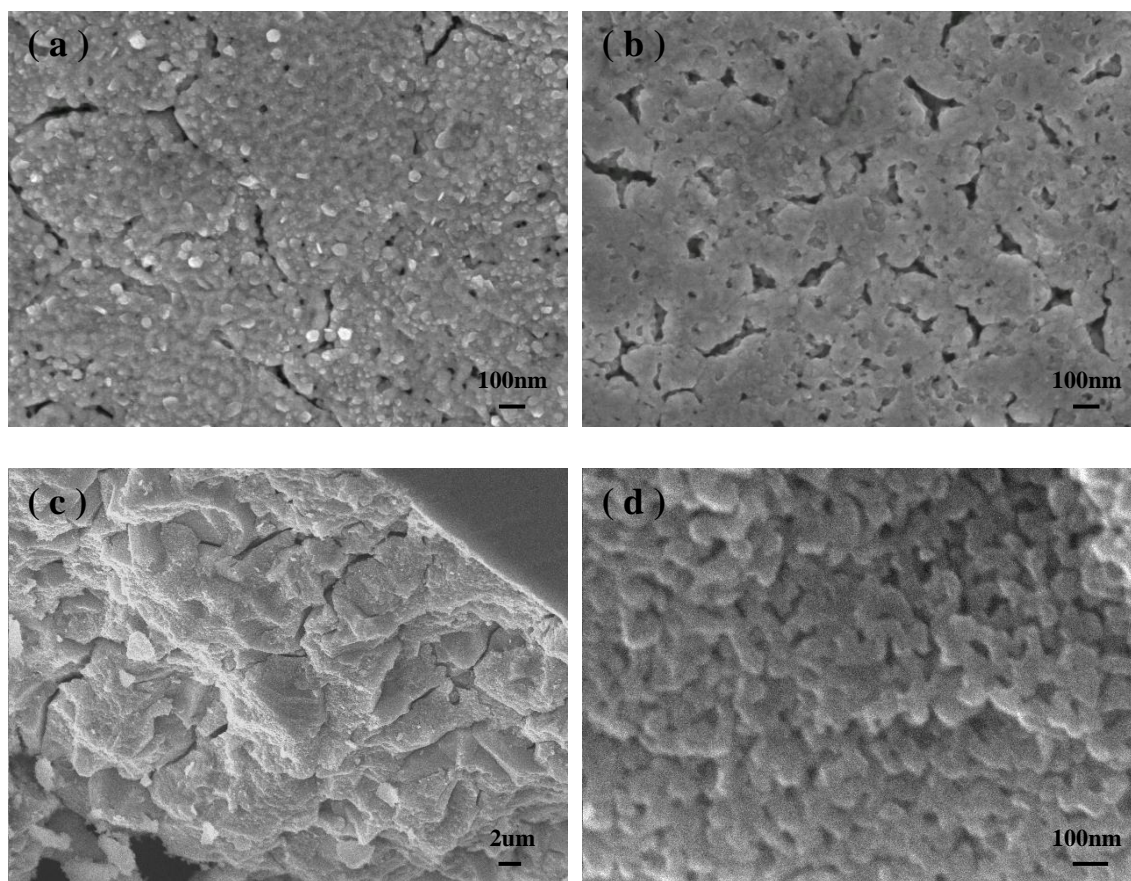


Figure 6. SEM images showing the microstructure of (a) free surface, (b) quenching surface, and (c, d) cross-section of the NPC ribbons by dealloying of the RS Mg-32 Cu alloy in the HCl solution for 30 min. (d) High-magnification image corresponding to part c.

In contrast, the coarsening process in the acidic solution of porous structure along the thickness direction of the NPC ribbons from Mg-32 Cu alloy during the post-dealloying is also further investigated herein. When the dealloying time reaches 30 min, there is no noticeable porous structure observed from the surfaces of samples, whereas there still exists an intact porous network in the interior, as presented in Figure 6. The phenomenological characteristic seems to be comparable to that upon the dealloying for 10 min described above; it should be noted that, however, there is an essential difference between their kinetic processes. The present results suggest that the coarsening process of porous structure along the thickness direction of samples during the post-dealloying is from the outside

to the inside, which is just contrary to the evolution process along the thickness direction during the dealloying. EDX analysis also has been performed on the surface and cross-section of the NPC ribbons, indicating that only Cu can be identified at this stage (not shown here).

Figure 7 shows Tafel polarization curves of single-phase α -Mg solid solution and Mg_2Cu intermetallic compound in the HCl solution, respectively. It can be found that the difference between free-corrosion potentials of the single-phase α -Mg and Mg_2Cu in the acidic solution is ~ 793 mV(SCE), which clearly indicates that the α -Mg have a relatively high electrochemical activity compared to the Mg_2Cu in the HCl solution.

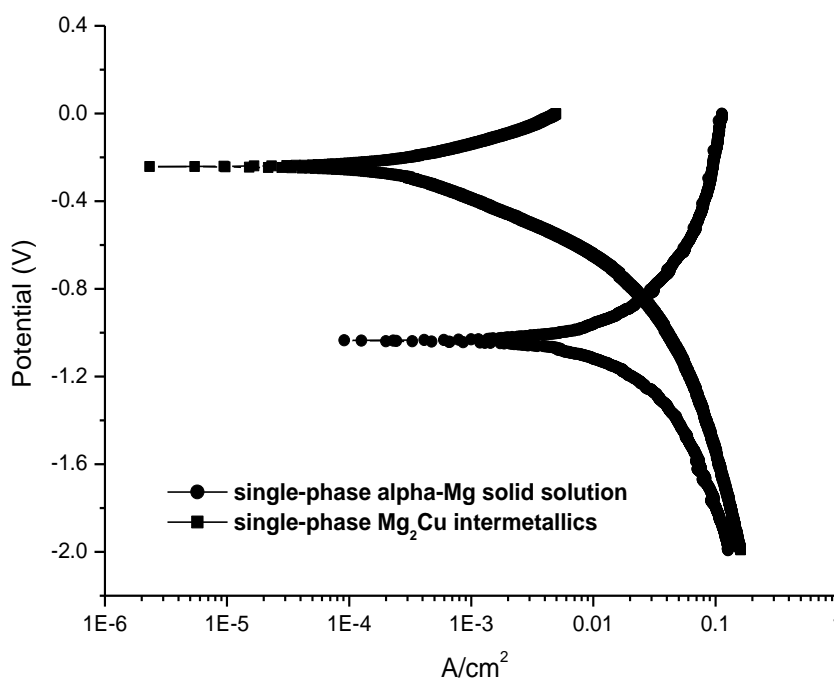


Figure 7. Tafel polarization curves of single-phase α -Mg solid solution and Mg_2Cu intermetallic compound in the HCl solution.

It is generally recognized that ideal bicontinuous nanoporous structures are obtained from binary alloy families with a single-phase solid solubility across all compositions by chemical/electrochemical dealloying. The formation mechanism of nanoporous structures during dealloying has been described in the literature [8]. It has been shown that ligaments form as a result of an intrinsic pattern formation during which aggregation of chemically driven noble metal atoms occurs. The process started with selective dissolution of base metal atoms from the outermost alloy surface, leaving behind noble metal atoms that diffused along alloy/solution interfaces and agglomerated into the ligaments. Thus, porosity evolution forms dynamically during dissolution and is not due to one active component simply being excavated out of a binary alloy [27].

However, if multiple phases exist in an alloy, a more complicated process will occur during dealloying. Typically, in a dual-phase alloy, if one phase can be dealloyed and another not, the alloy can be used to fabricate nanoporous metal composites, while if one phase is entirely dissolved and

another is partly corroded, the dealloying of the alloy can lead to NPMs with bimodal channel size distributions [28]. The present Mg-Cu alloy system is composed of a combination of α -Mg and Mg_2Cu . It is reasonable to assume that the dealloying of the RS Mg-Cu alloys could result into the formation of NPC with bimodal channel size distributions. In principle, the main disparity should just lie in the length scales of the large-sized channels in NPC depending upon the initial alloy composition, while those of smaller ones hardly could be influenced for a given dealloying solution, comparable to the case for NPG with bimodal channel size distributions [29]. Perplexingly, in actual fact, unlike the bimodal morphology of the NPG dealloyed from the Al-Au ribbons composed of two phases: α -Al and Al_2Au [29], the microstructures of NPC from the present Mg-13.5, 14.5, 15.5, 25 Cu alloys are homogeneous throughout the whole ribbons although the initial ribbons also contain similar-structure-typed two phases: α -Mg and Mg_2Cu . We consider that the synergetic dealloying of the coexisting α -Mg and Mg_2Cu in the dual-phase Mg-Cu alloys and the fast surface diffusion of Cu atoms along the alloy/solution interfaces result in the formation of NPC with a homogeneous porous structure. For the present Mg-Cu alloys, the electrochemical activity of α -Mg phase are much higher than that of Mg_2Cu as indicated in Figure 7. Thus, α -Mg and Mg_2Cu phases existing in the alloys can form corrosion couple cells, with the α -Mg (Mg-rich phase) acting as an anode and preferentially dissolving during dealloying compared to the Mg_2Cu . The preferential dissolution of α -Mg phase forms a large number of tiny paths like a 3D porous network for the penetration of the solution throughout the whole thickness of the ribbons and the dealloying of α -Mg facilitates that of Mg_2Cu , especially for the Mg-25 Cu alloy containing relatively more Mg_2Cu . Also, Mg can be selectively preferentially etched in the Mg_2Cu phase. Recently, Zhang et al. [30] have reported that the synergetic dealloying of α -Al and Ag_2Al in the dual-phase Al-Ag alloys and the fast surface diffusion of Ag atoms lead to the formation of NPS with a homogeneous porous structure. Obviously, the surface diffusivity of Cu in solution is on the order of $10^{-10} \text{ cm}^2 \cdot \text{s}^{-1}$, faster than that of Ag (on the order of $10^{-12} \text{ cm}^2 \cdot \text{s}^{-1}$), and much faster than that of Au (on the order of $10^{-14} \text{ cm}^2 \cdot \text{s}^{-1}$) [30,31]. Thus, it may be easier to understand that the synergetic dealloying of α -Mg and Mg_2Cu in the initial Mg-Cu alloys and the faster surface diffusion of Cu atoms should be responsible for the uniformity of the resultant nanoporous samples. It should be noted that, however, the as-dealloyed porous structure of the Mg-32 Cu alloy is significantly different from those of other Mg-Cu alloys. The NPC from the Mg-32 Cu alloy ribbons has bimodal channel size distributions composed of large-sized channels with highly porous channel walls. Thus, another mechanism can be postulated for the dealloying of the Mg-32 Cu alloy in the HCl solution at room temperature.

As indicated by the XRD results in Figure 1A, with the increase of Cu content in the initial alloys, the volume fraction of the Mg_2Cu phase continually increases, while a corresponding decrease is shown clearly in the α -Mg phase. For the RS Mg-32 Cu alloy, the much lower amount of α -Mg might result into the more difficult realization of the synergetic dealloying mechanism between the two distinct phases. Thus, it is reasonable to assume that α -Mg and Mg_2Cu in the dual-phase Mg-32 Cu alloy ribbons are more prone to be separately dealloyed, leading to the formation of NPC with bimodal channel size distributions. Obviously, this is in good agreement with the SEM observations, indicating that the microstructures of the NPC ribbons strongly depend upon the phase proportions of the initial

Mg-Cu alloys. In addition, it should be noted that the parting limit should exist between 25 and 32 at.% Cu for the dealloying of the Mg-Cu alloys in the HCl solution.

Moreover, for the NPC ribbons from the Mg-32 Cu alloy, it is worth noting that the microstructure of quenching surface is essentially different from that of the free surface. According to the Mg-Cu phase diagram [19], during the solidification of the quenching surface, primary Mg₂Cu phases precipitate firstly and the α -Mg solid solution subsequently forms from the remaining liquid, suppressing the occurrence of the eutectic reaction due to the fast cooling rate of the surface. The microstructure on the quenching surface can be described as the α -Mg phase surrounding the primary Mg₂Cu phase, namely divorced eutectic structure. In contrast, during the solidification of the free surface contacting with the air, the eutectic reaction can normally occur from the remaining liquid after the first precipitation of primary Mg₂Cu phase due to the relatively slow cooling rate. The α -Mg and Mg₂Cu phases co-exist in the eutectic structure on the free surface in the form of layered alternant distribution. During the etching, the excavation of the α -Mg phase out of the alloy contributes to the formation of large-sized channels in the NPC ribbons, while the dealloying of the Mg₂Cu phase results in the nanoporous structure of the large-sized channel walls. Obviously, different microstructures can be obtained on the two distinct surfaces upon the dealloying due to the different distribution states of α -Mg and Mg₂Cu phases. Thus, despite having the same composition, the free and quenching surfaces of the alloy ribbons take on different dealloying morphologies and we can conclude that the phase distributions of the initial alloys also have a key influence on the microstructures of the NPC ribbons. Moreover, the morphology, size, and orientation of the Mg₂Cu phase can be conserved into the resulting NPC ribbons. From the section-view and two distinct plane-view SEM images, we can further know the information of the α -Mg and Mg₂Cu phases in the initial RS Mg-32 Cu ribbons. In addition, the length scales of the large-sized channels in NPC can be modulated by simply changing the alloy composition of Mg-Cu because the amount of the α -Mg phase varies with tuning Cu concentration in the Mg-Cu alloys with Cu content between 25 and 33 at.% (up to 33 at.% Cu corresponding to a single-phase Mg₂Cu alloy).

It is well established that the evolution of porous structure during dealloying involves etching of the base metal coupled with coarsening of the noble metal by surface diffusion [10,28]. Based upon the percolation theory, dealloying would be only isolated to surface grains unless a mechanism exists for the percolation of the solution throughout the alloy [32]. In the present Mg-Cu alloys, at the initial stage of dealloying, the α -Mg phase dissolved preferentially can serve as percolating paths throughout the whole alloy ribbons, which facilitates the further occurrence of dealloying in the interior of ribbon. Besides, the large number of grain boundaries might permit the solution to penetrate through the corroded boundary into the interior. It has been reported that various kinds of nonequilibrium defects can be introduced into the lattice during rapid solidification, which constitute a high excess stored energy [16,29]. From a thermodynamic point of view, as a result, the driving force for the dissolution of Mg atoms in the interior of alloy is significantly enhanced. Porosity evolution forms dynamically during dissolution [29]. Thus, the faster dissolution of Mg atoms results in the preferential formation of porous network in the interior. This is why upon the dealloying for 10 min, a well-evolved porous structure can be obtained in the interior of samples while no noticeable counterparts can be observed on the surfaces.

It has been acknowledged that, during the post-dealloying, surface diffusion of noble metal element along the alloy/solution interfaces plays a key role in the coarsening of NPMs and has a significant influence on length scales of ligaments [8,27]. As the dealloying time increased from 15 min up to 30 min, nanoporous structure of the NPC ribbons from the Mg-32 Cu alloy gradually coarsens due to the Ostwald ripening effects [33]. Intriguingly, the coarsening rate of the nanoporous structure along the thickness direction of samples is markedly different, indicative of substantial coarsening with greater diffusivity on the surfaces, as discussed in detail in the following part.

It was reported that the surface diffusivity in solution of Cu atoms along alloy/solution interfaces is generally of order of $10^{-10} \text{ cm}^2 \text{ s}^{-1}$, and the adsorption of chloride ion (Cl^-) in HCl solution can greatly enhance the surface diffusion of Cu atoms during the dealloying [28,34]. As far as given dealloying solutions and alloy systems are concerned, surface diffusion of noble metal element along alloy/solution interfaces strongly depends upon dealloying solution concentration [8,27,35-37], and that is just the adsorbed Cl^- concentration in the present case. It might remarkably modify the enthalpy and entropy of formation of surface moving entities and adsorbed bonds between neighboring sites due to electron transfer reactions [38,39]. Obviously, adsorbed Cl^- concentration on the surfaces of samples is much higher than that in the interiors because nano-scaled channels near the top surface severely restrict the transport of ions into the inner space of the structure [40]. Thus, the diffusivity of Cu atoms on the surfaces of samples can be significantly enhanced, and this is why upon the dealloying for 30 min, the porous structure on the surface of the NPC ribbons has coarsened into the plane-like morphology, while the intact porous characteristics still exist in the interior. From a dynamical point of view, we can conclude that the evolution process of porous structure along the thickness direction of samples during the dealloying is kinetically controlled by the dissolution of Mg atoms, while the coarsening process during the post-dealloying by the diffusion of Cu atoms.

The nonmonolithic characteristic of Raney metals is inconsequential to their applications as a catalyst because the main property required is high surface area. However, the mechanical integrity of NPMs is important for their structural properties and some applications because uniformity and continuity are key requirements. For the present Mg-13.5, 14.5, and 15.5 Cu alloys, it should be noted that despite the monolithic characteristic upon dealloying, the NPC ribbons are brittle and soft, and their shape cannot be well preserved compared to that obtained by the dealloying of Mg-25 Cu. Moreover, we found cracking to be unavoidable in these as-dealloyed samples upon the dealloying. For the Mg-32 Cu alloy, although a few minor cracks still can be observed on the surfaces of the as-dealloyed ribbons, the present NPC ribbons with bimodal channel size distributions are monolithic and can be handled and loaded. These NPC ribbons can serve as model materials to investigate the mechanical, physical, and chemical properties associated with random porous structure of nanoporous solids. In addition, it is reasonable to assume that with the increase of content of the more noble metal element in the initial alloy ribbons, the mechanical property of NPMs can be improved accordingly. This will be discussed detailedly in a separate paper.

As indicated above, it is generally recognized that NPMs with ideal bicontinuous structures are obtained from binary alloys with a single-phase solid solubility across all compositions (like Ag-Au, Mn-Cu, etc.) [8,14]. Erlebacher [27] described a kinetic Monte Carlo model to well explain the underlying physical mechanism of dealloying of Ag-Au solid solution alloys and nanoporosity

evolution. However, some researchers have cast doubts that the model can describe the dealloying process of intermetallic compounds due to their complex structures, such as Al_3Pd , Ag_2Al , Al_2Cu , and the like [36,41-43]. Parida and co-workers [25] have reported that the dealloying of Ag-Au, such as $\text{Ag}_{70}\text{Au}_{30}$, does not require either nucleation of new crystallites or the formation/removal of lattice sites. On a basis of the present results, it is obvious that the crystal nucleation and formation/removal of lattice sites should be necessary during the dealloying of Mg_2Cu intermetallic compound. Recently, Zhang et al. [44] have also argued that a more complicated mechanism, e.g., nucleation and growth instead of spinodal decomposition, is required for the Au atoms in the initial monoclinic AlAu lattice to reconstruct the f.c.c. structure of Au. Obviously, these deep-seated issues still need to be further investigated.

Based on our present work, it can be proposed that the further investigations on the dealloying behavior of Mg_2Cu in the Mg-Cu alloys in the acidic solution will have important implications for understanding the underlying physical mechanism of dealloying of intermetallic compounds. More importantly, we can effectively achieve the tailoring of nanoporous structure, such as surface morphology and ligament/channel sizes, via controlling the dealloying behavior among different phases in these multi-phase, low-cost alloys with a broad composition range and thus lay a solid foundation for their original applications in lithium ion batteries within the green, new energy industry. Some encouraging test findings have been obtained in our previous work [45-46], the extensive study is in progress.

4. CONCLUSION

Monolithic NPC ribbons with single modal or bimodal channel size distributions can be fabricated through chemical dealloying of Mg-Cu alloys with Cu content below 33 at.% in the HCl solution at room temperature. With increasing Cu content from 13.5 at.% up to 32 at.%, NPC with unimodal channel size distributions gradually changes into that with bimodal channel size distributions upon the dealloying; meanwhile we found cracking to be unavoidable. For the Mg-Cu alloys composed of $\alpha\text{-Mg}$ and Mg_2Cu , the microstructure of the NPC ribbons strongly depends upon the phase proportions and distributions in the initial alloys. The Mg-13.5~25 Cu alloys with a certain amount of $\alpha\text{-Mg}$ can be fully dealloyed and result in the formation of NPC with a homogenous structure in virtue of the synergetic dealloying of $\alpha\text{-Mg}$ and Mg_2Cu and the fast surface diffusion of Cu atoms. The separate dealloying of $\alpha\text{-Mg}$ and Mg_2Cu in the Mg-32 Cu alloy leads to the formation of NPC with bimodal channel size distributions due to the much low amount of $\alpha\text{-Mg}$ in the initial alloy. Moreover, the microstructures of two distinct surfaces of the NPC ribbons from Mg-32 Cu alloy make an essential difference due to the different distribution states of $\alpha\text{-Mg}$ and Mg_2Cu dependent on the cooling rates of the free and quenching surfaces during rapid solidification. Additionally, the evolution process of porous structure along the thickness direction of the alloy ribbons during the dealloying is from the interior to the exterior, which is related to the faster dissolution rate of Mg atoms in the interior. Contrarily, the coarsening of porous structure during the post-dealloying can be described as a

process from the outside to the inside of the NPC ribbons, which can be attributed to the greater diffusivity of Cu atoms on the surfaces induced by the higher absorbed Cl⁻ concentration.

ACKNOWLEDGEMENT

We give thanks to financial support by the State Key Basic Research Program of PRC (2007CB936502), the National Natural Science Foundation of China (50574008, 50954005, 51074011), and the National 863 Program Project (2006AA03Z230, 2008AA03Z208). Also, we are grateful to Prof. T. Zhang and Dr. J.F. Wang for assistance in preparation of the starting alloy ribbons. W.B. Liu thanks Prof. Z.H. Zhang (Shandong University) for useful discussions.

References

1. G. C. Bond and D. T. Thompson, *Catal. Rev.*, 41 (1999) 319.
2. T. You, O. Niwa, M. Tomita and S. Hirono, *Anal. Chem.*, 75 (2003) 2080.
3. J. R. Weissmueller, N. Viswanath, D. Kramer, P. Zimmer, R. Wuerschum and H. Gleiter, *Science*, 300 (2003) 312.
4. S. H. Joo, S. J. Choi, K. J. Kwa and Z. Liu, *Nature*, 412 (2001) 169.
5. H. Masuda and K. Fukuda, *Science*, 268 (1995) 1466.
6. G. S. Attard, P. N. Bartlett, N. R. B. Coleman, J. M. Elliott, J. R. Owen and J. H. Wang, *Science*, 278 (1997) 838.
7. T. Kijima, T. Yoshimura, M. Uota, T. Ikeda, D. Fujikawa, S. Mouri and S. Uoyama, *Angew. Chem., Int. Ed.*, 43 (2004) 228.
8. J. Erlebacher, M. J. Aziz, A. Karma, N. Dimitrov and K. Sieradzki, *Nature*, 410 (2001) 450.
9. K. Sieradzki, N. Dimitrov, D. Movrin, C. McCall, N. Vasiljevic and J. Erlebacher, *J. Electrochem. Soc.*, 149 (2002) B370.
10. C. X. Ji and P. C. Searson, *J. Phys. Chem. B*, 107 (2003) 4494.
11. M. Stratmann and M. Rohwerder, *Nature*, 410 (2001) 420.
12. D. V. Pugh, A. Dursun and S. G. Corcoran, *J. Electrochem. Soc.*, 152 (2005) B455.
13. U. S. Min and J. C. M. Li, *J. Mater. Res.*, 9 (1994) 2878.
14. B. W. Parks Jr., J. D. Fritz and H. W. Pickering, *Scripta Mater.*, 23 (1989) 951.
15. J. Snyder, P. Asanithi, A. B. Dalton and J. Erlebacher, *Adv. Mater.*, 20 (2008) 4883.
16. H. B. Lu, Y. Li and F. H. Wang, *Scripta Mater.*, 56 (2007) 165.
17. D. V. Pugh, A. Dursun and S. G. Corcoran, *J. Electrochem. Soc.*, 152 (2005) B65.
18. C. C. Zhao, Z. Qi, X. G. Wang and Z. H. Zhang, *Corrosion Sci.*, 51 (2009) 2120.
19. J. L. Murray, H. Okamoto and T. B. Massalski, *Bull. Alloy Phase Diagrams*, 8 (1987) 20.
20. M. Raney, *U.S. Patent No. 1563587*, (1925).
21. M. C. Dixon, T. A. Daniel, M. Hieda, D. M. Smilgies, M. H. W. Chan and D. L. Allara, *Langmuir*, 23 (2007) 2414.
22. K. Sieradzki, R. R. Corderman and K. Shukla, *Phil. Mag. A*, 59 (1989) 713.
23. Y. Ding, A. Mathur, M. W. Chen and J. Erlebacher, *Angew. Chem., Int. Ed.*, 44 (2005) 4002.
24. Y. Ding, Y. J. Kim and J. Erlebacher, *Adv. Mater.*, 16 (2004) 1897.
25. S. Parida, D. Kramer, C. A. Volkert, H. Rössner, J. Erlebacher and J. Weissmüller, *Phys. Rev. Lett.*, 97 (2006) 035504.
26. A.J. Forty and P. Durkin, *Philos. Mag. A*, 42 (1980) 295.
27. J. Erlebacher, *J. Electrochem. Soc.*, 151 (2004) C614.

28. Z. Qi, C. C. Zhao, X. G. Wang, J. K. Lin, W. Shao, Z. H. Zhang and X. F. Bian, *J. Phys. Chem. C*, 113 (2009) 6694.
29. Z. H. Zhang, Y. Wang, Z. Qi, J. K. Lin and X. F. Bian, *J. Phys. Chem. C*, 113 (2009) 1308.
30. X. G. Wang, Z. Qi, C. C. Zhao, W. M. Wang and Z. H. Zhang, *J. Phys. Chem. C*, 113 (2009) 13139.
31. N. Hirai, H. Tanaka and S. Hara, *Appl. Surf. Sci.*, 506 (1998) 130.
32. D. V. Pugh, A. Dursun and S.G. Corcoran, *J. Mater. Res.*, 18 (2003) 216.
33. A.M. Hodge, J. Biener, J. R. Hayes, P. M. Bythrow, C. A. Volkert and A. V. Hamza, *Acta Mater.*, 55 (2007) 1343.
34. W. B. Liu, S. C. Zhang, N. Li, J. W. Zheng and Y. L. Xing, *J. Electrochem. Soc.*, 157 (2010) D666.
35. W. B. Liu, S. C. Zhang, N. Li, J. W. Zheng and Y. L. Xing, *Microporous Mesoporous Mater.*, 138 (2011) 1.
36. Z. H. Zhang, Y. Wang, Z. Qi, W. H. Zhang, J. Y. Qin and J. Frenzel, *J. Phys. Chem. C*, 113 (2009) 12629.
37. Z. H. Zhang, Y. Wang, Y. Z. Wang, X. G. Wang, Z. Qi, H. Ji and C. C. Zhao, *Scripta Mater.*, 62 (2010) 137.
38. J. M. Dona and J. Gonzalez-Velasco, *Surf. Sci.*, 274 (1992) 205.
39. J. M. Dona and J. Gonzalez-Velasco, *J. Phys. Chem.*, 97 (1993) 4714.
40. H. C. Shin and M. L. Liu, *Chem. Mater.*, 16 (2004) 5461.
41. W. B. Liu, S. C. Zhang, N. Li, J. W. Zheng and Y. L. Xing, *Corrosion Sci.*, 53 (2011) 809.
42. W. B. Liu, S. C. Zhang, N. Li, J. W. Zheng and Y. L. Xing, *J. Electrochem. Soc.*, 158 (2011) D91.
43. W. B. Liu, S. C. Zhang, N. Li, J. W. Zheng and Y. L. Xing, *J. Electrochem. Soc.*, 158 (2011) D611.
44. Q. Zhang, X. G. Wang, Z. Qi, Y. Wang and Z. H. Zhang, *Electrochimica Acta*, 54 (2009) 6190.
45. S. C. Zhang, Y. L. Xing, W. B. Liu, and J. W. Zheng, *The 15th International Meeting on Lithium Batteries, IMLB*, J. Electrochem. Soc., Abstract #82, Montréal, Canada, June 27-July 2, (2010).
46. S. C. Zhang, Y. L. Xing, T. Jiang, Z. J. Du, F. Li, L. He and W. B. Liu, *J. Power Sources*, 196 (2011) 13963.